SOH analysis of Li-ion battery based on ECM parameters and broadband impedance measurements

1st Jussi Sihvo
Department of Electrical Engineering
Tampere University
Tampere, Finland
jussi.sihvo@tuni.fi

2nd Tomi Roinila
Department of Electrical Engineering
Tampere University
Tampere, Finland
tomi.roinila@tuni.fi

3th Daniel-Ioan Stroe
Department of Energy Technology
Aalborg University
Aalborg, Denmark
dis@et.aau.dk

***Abstract*—The impedance of a Li-ion battery is an important parameter for the battery state-of-health (SOH) estimation. The dependency of the battery impedance to the SOH can be monitored by fitting an equivalent-circuit-model (ECM) to the impedance data and observe the changes in the ECM parameters. The ECM is typically fitted by the complex-non-linear-least-squares (CNLS) algorithm which requires accurately chosen initial conditions for the parameters to guarantee the consistent performance of the algorithm. In order to use the ECM parameters for SOH estimation in practical applications, the impedance measurements should be fast and simple to implement to the battery system. This paper demonstrates the utilization of practical and fast pseudo-random-sequence (PRS) impedance measurements to the SOH analysis of a nickel manganese cobalt Li-ion battery by observing the variations in the ECM parameters. The measured impedances are fitted to the ECM by using the CNLS with adaptively obtained initial conditions. It is shown that the ECM parameters are changing as the battery capacity degrades. In addition, it is observed that some parameters are able to indicate a drastic reduction in the battery capacity and SOH.**

***Index Terms*—Li-ion batteries, PRS, practical impedance measurements, SOH, State-estimation**

I. Introduction

Lithium-ion (Li-ion) batteries are widely recognized as a state-of-the-art solution for energy storages in electrical transportation and renewable energy source applications [1]. Li-ion battery storages are usually equipped with a battery management system that actively monitors the state-of-charge (SOC) and the state-of-health (SOH) of the battery. These parameters are typically estimated indirectly by voltage, current and temperature measurements [2], [3].

As the Li-ion battery ages, the electrochemical properties of the battery cell are weakened which leads to capacity and power fade and reduction in the SOH [4]–[7]. Typical aging effects in the Li-ion batteries are the lithium-plating and the growth of SEI-layer which are leading to capacity and power fade in the Li-ion batteries. In addition, corrosion of the electrodes and current collectors are increasing the capacity and power fade. In general, high temperatures, overcharging/discharging and too low/high SOC levels are accelerating these effects [4]. In addition, the lithium plating effect is increased at low temperatures with high cycling rates. Moreover, these effects are often simultaneously taking place and many of them are difficult to identify accurately. These aspects significantly complicates the accuracy of the SOH estimation in battery applications.

Recent studies have shown that the impedance of a Li-ion battery has a strong dependency on the battery SOH [5]–[7]. A common approach for obtaining the battery impedance is applying electrochemical-impedance-spectroscopy (EIS) where a sinusoidal perturbation is applied to the battery current [8]. The method provides accurate impedance information but is difficult to be implemented in practical on-board applications as it is slow and complex. An interesting alternative is to use broadband pseudo-random-sequence (PRS) signals [9]–[11]. The PRS methods are simple to implement and capable for producing fast impedance measurements but their performance is often limited for non-linear systems. However, some PRS signals can be designed to reduce the effect of the nonlinear distortion [10], [11]. One of such signals is the direct-synthesis-ternary (DST) sequence which is reported to provide accurate measurements in specific non-linear system case studies [11].

In order to study the dependency between the battery impedance and the SOH, the measured impedance should be fitted to the non-linear equivalent-circuit-model (ECM) parameters [12]–[15]. The complex-non-linear-least-squares (CNLS) method is typically used to fit the impedance data [6], [13], [16]. However the CNLS method requires initial conditions for the ECM parameters which should be appropriately chosen to guarantee the consistent fitting results. The initial conditions can be provided based on the shape of the impedance in the complex plane [12], [14], [15]. A systematic approach to provide the initial conditions for all ECM parameters is presented in [15]. The approach works adaptively and is well scalable to impedances of different battery chemistries and, therefore, is useful for practical implementation of the ECM fitting for the SOH analysis.

This work demonstrates the use of ECM parameters and practical impedance measurements for the SOH analysis of the nickel-manganes-cobalt (NMC) Li-ion battery cell. The battery cell is cycled by the Worldwide-harmonized-Light-duty-driving-Test-Cycle (WLTC) profile which provides realistic charge/discharge profile for the battery cycling. The battery performance is occasionally tested during the WLTC tests with

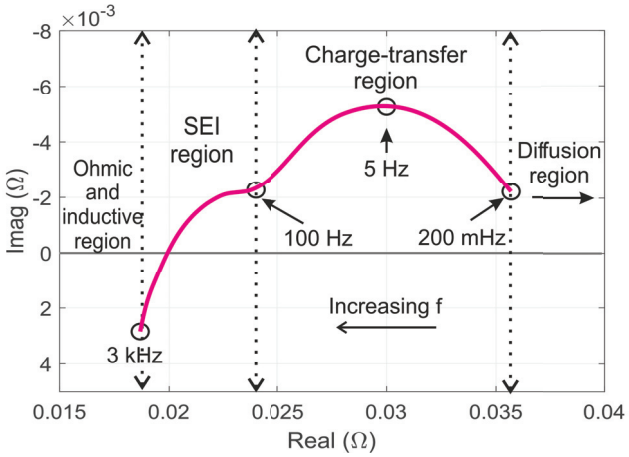

Fig. 1: Impedance plot of a NMC battery cell

capacity measurements and impedance measurements based on the DST sequence. The CNLS algorithm with adaptively obtained initial conditions are used to fit the non-linear ECM to the impedance measurements. The results show that the ECM is accurately fitted throughout the experiments to the impedance data. In addition, it is shown that the ECM parameters are increasing as the battery capacity and SOH are decreasing. Therefore, applying the impedance measurement along with the ECM parameters provides a highly potential tool for reliable SOH estimation in on-board battery applications.

The rest of the paper is organized as follows. The applied impedance ECM model is presented in Section II and the proposed fitting algorithm is introduced in Section III. The impedance measurements and DST sequence design are presented in Section IV. The experiments and the results are presented in Sections V and VI, respectively. Conclusions are drawn in Section VII.

II. Impedance Model

A typical impedance of a Li-ion NMC cell is shown in Fig. 1. In the impedance plot, different regions can be identified. Each region is formed by different electrochemical processes in the battery cell. The impedance shape consists of two semicircles. The first one at low frequencies is the charge-transfer region describing the charge-transfer and electrochemical double-layer reactions The second one, more indistinguishable semicircle at the middle frequencies is formed by the solid-electrolyte-interface (SEI) effect which is caused by the layer developing at the surface of the electrodes. The ohmic and inductive region is formed by the resistance and inductance of the current collectors, electrodes, and wirings and is generally affecting the high frequencies above 1 kHz. [4], [5], [13]

A non-linear ECM for the studied NMC-cell is shown in Fig. 2 and its mathematical representation is given in (1). The ECM utilizes a non-linear constant-phase-element (CPE) given

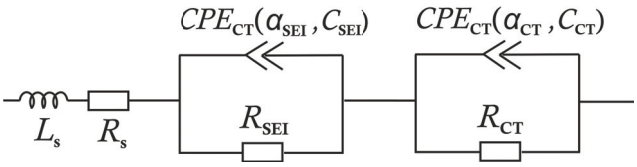

Fig. 2: Suitable ECM for the used NMC cell

in (2) where C is the capacitance and α is the suppression factor having values between 0 and 1 [12]–[15]. The charge-transfer and SEI region impedances Z_{SEI} and Z_{CT} are modeled by a parallel connection of a resistor and CPE which are given in (3). The impedance at the ohmic and inductive region can be modeled by a series resistor R_{s} and an inductor L_{s}.

$$Z_{\text{NMC}} = j\omega L_{\text{s}} + R_{\text{s}} + Z_{\text{SEI}} + Z_{\text{CT}} \tag{1}$$

$$Z_{\text{CPE}} = \frac{1}{(j\omega)^{\alpha} C}, \tag{2}$$

$$Z_{\text{CT}} = \frac{1}{\frac{1}{R_{\text{CT}}} + (j\omega)^{\alpha_{\text{CT}}} C_{\text{CT}}}, Z_{\text{SEI}} = \frac{1}{\frac{1}{R_{\text{SEI}}} + (j\omega)^{\alpha_{\text{SEI}}} C_{\text{SEI}}} \tag{3}$$

The aging phenomenons of the battery have an effect on the shape of the battery impedance [4]–[7], [17]. Typical aging effects, such as, lithium plating, SEI-layer formation and corrosion of the current collectors, are generally increasing the series resistance R_{s} of the impedance. The SEI-layer formation also affects on the SEI-region by changing the semicircle and, thus, the parameters of Z_{SEI}. The charge-transfer region impedance Z_{CT} is affected by both the SEI formation and the lithium-plating. Although these aging phenomena are more or less mixed in the impedance curve, the relative effect of the SOH on the ECM parameters can be investigated by tracking the variations in these parameters throughout the battery life.

III. ECM Initialization and Fitting

In order to fit the ECM to the battery impedance data, a fitting algorithm, such as, the complex-non-linear-least-squares (CNLS) algorithm can be used [16]. The CNLS requires a selection of initial conditions for the ECM parameters which should be relatively accurately chosen. As the ECM parameters changes along the battery aging, the initial values should be adaptively chosen to guarantee consistent performance for the CNLS in all operating conditions. Appropriate initial conditions can be extracted by utilizing the shape of the impedance curve [12]–[15]. In this paper, the initialization is mostly based on the methods presented in [15].

Fig. 3 illustrates the location of the important points in the impedance data which are utilized to extract the initial conditions. These points are the minimum derivative point in the SEI region ($R_{\text{D-SEI}}$, $X_{\text{D-SEI}}$) and zero-derivative point in the charge-transfer region ($R_{\text{D-CT}}$, $X_{\text{D-CT}}$). In addition, the minimum real part of the impedance (R_{minreal}, X_{minreal}) and the first data point in the impedance data ($Z(1)$) are utilized

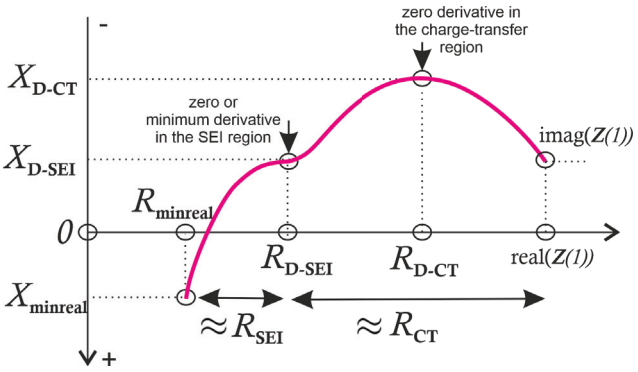

Fig. 3: Illustration of the specific points in the impedance curve for the extraction of the ECM parameters

for the initialization. To simplify the extraction process, each part in the impedance in (1) is individually extracted.

The initial conditions for the series resistance R_{SEI} and R_{CT} are approximated by the width of the corresponding semicircles which, from Fig. 3, can be given as in (4) and (5). The suppression factors are extracted based on the fact that, for the parallel connection of the resistor R and CPE (ω, C, α), the impedance in the top of the semicircle is independent of the frequency and capacitor values [15]. Moreover, the real and imaginary parts of the impedance have a relation given in (6) [15]. The suppression factor α_{SEI} and α_{CT} can then be solved from (6) as given in (7) and (8). As there is no semicircle top in the SEI-region, (8) is approximated by the extracted minimum derivative point in this case.

The capacitor values can then be initialized by separating the real parts of Z_{SEI} and Z_{CT} in (3) and arranging it in terms of C_{SEI} and C_{CT}, respectively. The data points and frequencies corresponding the extracted $R_{\text{D-SEI}}$ and $R_{\text{D-CT}}$ should be used for the calculations. The obtained coefficients given in (9) and (10), can then be substituted to (11) to solve C_{SEI} and C_{CT}. [15]

$$R_{\text{CT}} = \text{real}(Z(1)) - R_{\text{D-SEI}} \tag{4}$$

$$R_{\text{SEI}} = R_{\text{D-SEI}} - R_{\text{minreal}} \tag{5}$$

$$X = \frac{R\sin(\frac{\pi\alpha}{2})}{2(\cos(\frac{\pi\alpha}{2})+1)} \tag{6}$$

$$\alpha_{\text{CT}} = \frac{4}{\pi}\text{atan}(\frac{X_{\text{D-CT}}}{\frac{R_{\text{CT}}}{2}}) \tag{7}$$

$$\alpha_{\text{SEI}} = \frac{4}{\pi}\text{atan}(\frac{X_{\text{D-SEI}}}{\frac{R_{\text{SEI}}}{2}}) \tag{8}$$

$$C_{\text{CT}} \rightarrow \begin{cases} a = (R_{\text{D-CT}} - R_{\text{D-SEI}}){R_{\text{CT}}}^2\omega_{\text{D-CT}}^{2\alpha_{\text{CT}}} \\ b = \cos(\frac{\pi\alpha_{\text{CT}}}{2})R_{\text{CT}}\omega_{\text{D-CT}}^{\alpha_{\text{CT}}}(2(R_{\text{D-CT}} - R_{\text{D-SEI}}) - R_{\text{CT}}) \\ c = R_{\text{D-CT}} - R_{\text{CT}} - R_{\text{D-SEI}} \end{cases} \tag{9}$$

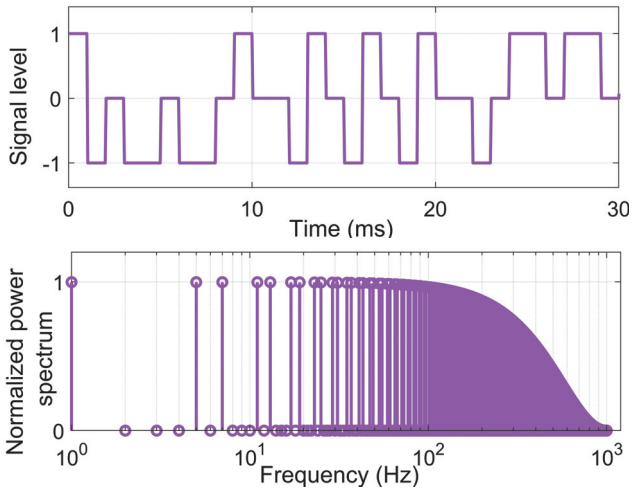

Fig. 4: Time and frequency-domain representation of the DST signal (N =1002, f_{gen} =1 kHz)

$$C_{\text{SEI}} \rightarrow \begin{cases} a = (R_{\text{D-SEI}} - R_{\text{minreal}}){R_{\text{SEI}}}^2\omega_{\text{D-SEI}}^{2\alpha_{\text{SEI}}} \\ b = \cos(\frac{\pi\alpha_{\text{SEI}}}{2})R_{\text{SEI}}\omega_{\text{D-SEI}}^{\alpha_{\text{SEI}}}R_{\text{SEI}} \\ c = R_{\text{SEI}} - R_{\text{SEI}} \end{cases} \tag{10}$$

$$C = \frac{-b - \sqrt{b^2 - 4ac}}{2a} \tag{11}$$

For the extraction of series resistance and inductance, the minimum real part impedance point is utilized. In this case, the SEI-region should also be taken into account as it has considerable effect on the impedance at high frequencies. By separating the real and imaginary parts of $R_{\text{s}} + j\omega L_{\text{s}} + Z_{\text{SEI}}$, the series resistance can be solved from the real part and inductance from the imaginary part as given in (12) and (13). [15]

$$R_{\text{s}} = R_{\text{minreal}} - \frac{R_{\text{SEI}} + \cos(\frac{\pi\alpha_{\text{SEI}}}{2})R_{\text{SEI}}^2 C_{\text{SEI}}\omega_{\text{minreal}}^{\alpha_{\text{SEI}}}}{1 + \cos(\frac{\pi\alpha_{\text{SEI}}}{2})R_{\text{SEI}}^2 C_{\text{SEI}}\omega_{\text{minreal}}^{\alpha_{\text{SEI}}} + (\omega_{\text{minreal}}^{\alpha_{\text{SEI}}}R_{\text{SEI}}C_{\text{SEI}})^2} \tag{12}$$

$$L_{\text{s}} = \frac{X_{\text{minreal}}}{\omega_{\text{minreal}}} + \frac{\sin(\frac{\pi\alpha_{\text{SEI}}}{2})R_{\text{SEI}}^2 C_{\text{SEI}}\omega_{\text{minreal}}^{\alpha_{\text{SEI}}}}{(\omega_{\text{minreal}} + 2\cos(\frac{\pi\alpha_{\text{SEI}}}{2})R_{\text{SEI}}C_{\text{SEI}}\omega_{\text{minreal}}^{\alpha_{\text{SEI}}+1} + (\omega_{\text{minreal}}^{\alpha_{\text{SEI}}+1}R_{\text{SEI}}C_{\text{SEI}})^2} \tag{13}$$

IV. Impedance Measurements

In this paper, the battery impedance measurements are carried out by perturbating the battery by a direct-synthesis-ternary (DST) signal [11]. The DST signal is a broadband signal which provides fast measurements and is simple to implement in practical application due to only three required signal levels. In addition, the method tends to suppress the effect of system non-linearities, thus, providing more accurate estimate of the underlying linear dynamics [10], [11].

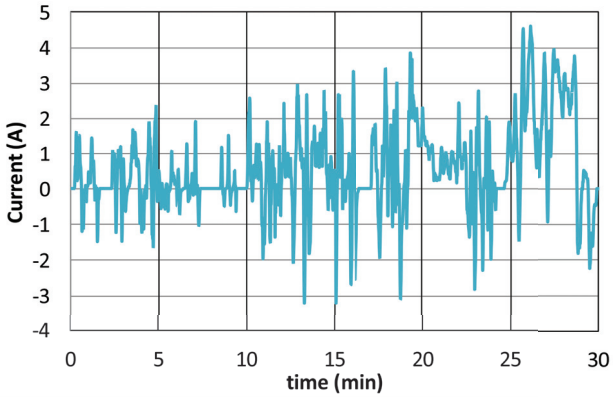

Fig. 5: WLTC current profile used for the battery cyclic aging

Fig. 4 illustrates the time and frequency domain characteristics of an example DST sequence. The signal length is 1002 and it is generated at 1 kHz. In the frequency domain, the signal has zero power at harmonic multiples of two and three which reduces the effect of second- and third-order non-linearities in the measurements [10], [11]. There are no sudden changes in the spectral power and the signal harmonics have power up to the generation frequency [9]. The DST signal can be generated according to the generation algorithm presented in [11].

The sequence length N and the sequence generation frequency f_{gen} determine the frequency resolution of the measurements as given in (14) which is also the lowest frequency harmonic that is measured. Due to the reduction in the signal power towards higher frequencies, the highest frequency that can be measured with the signal is approximately as given in (15) [9].

$$f_{\text{min}} = f_{\text{res}} = \frac{f_{\text{gen}}}{N}. \tag{14}$$

$$f_{\text{max}} = 0.45 * f_{\text{gen}}. \tag{15}$$

Eqs. (14) and (15) define the DST signal parameters that are required to cover the designed bandwidth of the impedance measurements [9]. The bandwidth for the battery measurements is determined by the battery impedance characteristics. The comprehensive characterization of very low frequencies (below 100 mHz) is avoided because this significantly increases the measurement time, which should be kept tolerable for practical applications. In addition, very high frequencies (above 5 kHz) are also avoided to keep the parameters for the DST measurements in (14) within tolerable limits for practical implementation. Another important design parameter is the amplitude of the sequence, which is the battery current.

TABLE I: DST signal design parameters for the measurements

amplitude	f_{gen}	N	bandwidth (f_{min} - f_{max})
2A	6kHz	32826	180 mHz - 2.7 kHz

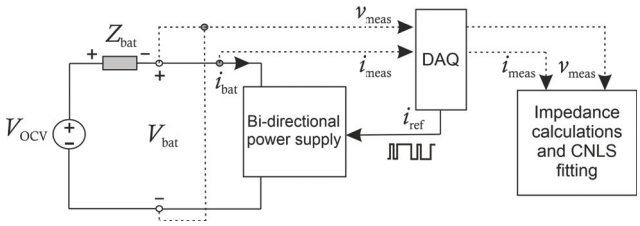

Fig. 6: Measurement setup for the battery impedance measurements

As the battery impedance is usually very small, the current should be relatively high in order to provide an appropriate signal-to-noise ratio for the measurements. The amplitude should also be low enough to prevent additional non-linear effects corrupting the measurements. As the magnitude of the impedance depends on the battery chemistry, the amplitude is often experimentally chosen.

V. Experiments

In the experiments, a Li-ion NMC battery cell with a nominal voltage of 4.2V and a capacity of 1.5Ah was exposed to a cyclic aging. In order to introduce a realistic aging for the battery cell, the Worldwide-harmonized-Light-duty-driving-Test-Cycle (WLTC) was used as the cycling profile. The WLTC is a driving profile of an electric vehicle which is scaled to corresponding current of the battery cell. A 30-minute-long WLTC current profile shown in Fig. 5 is used for the experiments as follows: A fully charged cell is discharged to 90% of SOC and applied by three consecutive WLTC profiles which consumes a total capacity of 0.9Ah from the battery cell. The battery cell is then fully discharged and charged again with a current of 0.5C for the next full WLTC cycle.

The experimental setup for the battery capacity and impedance measurements is illustrated in Fig. 6. The DST signal design parameters are given in Table I. The DST signal was injected from the DAQ device to the battery as the current reference of the bi-directional power supply. The current and voltage of the battery were measured and collected through the DAQ device and Fourier transform was used to obtain the battery impedance which was then applied to the ECM fitting. The impedance measurements were carried out with zero offset current to keep the SOC constant. The measurements were carried out with a 10% SOC resolution between 10%-90%. A relaxation time of 1 minute was considered before each impedance measurement. The resulting impedance spectra were filtered by moving-average-filter (MAF) to smooth the resulting spectra for the ECM fitting [18]. The amount of data was reduced by taking 150 logarithmically spaced data points from the impedance measurements. The temperature for the measurements was kept constant at 25°C throughout the experiments. In addition, the capacity of the cell was measured according to Coulomb counting method [2].

All of the measured impedances were fitted to an ECM by the CNLS algorithm with initial values calculated according

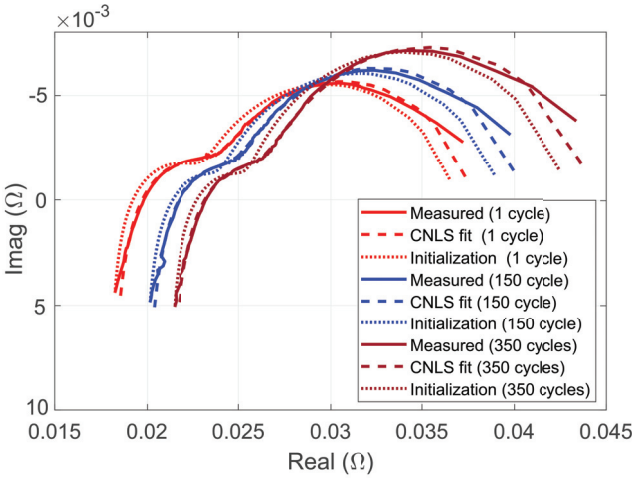

Fig. 7: Measured and fitted impedances at different aging conditions at 50% of SOC

to Section III. The SOH was defined in terms of capacity degradation of the battery with respect to the capacity at the beginning of the experiments (Q_0) as given in (16).

$$\mathrm{SOH}_i = \frac{Q_i}{Q_0} \tag{16}$$

VI. Results

Fig. 7 shows that the CNLS fits the ECM accurately to the impedance measurements. The initialization method provides relatively accurate fit and it can be considered as an efficient method to obtain the initial conditions for the CNLS. The largest error in the CNLS fits can be seen on the few first data points in the data at the charge-transfer region. This is caused by the fact that the frequency resolution of the measurement for this part of the impedance spectrum is too low to cover the semicircle shape sufficiently. Nevertheless, the fits are regarded to provide consistent ECM parameter values for the SOH analysis of the battery.

The fitted ECM parameters as a function of WLTC cycles are shown in Fig. 8. The most consistent dependency can be seen in the series inductance and resistances which is most likely caused by the corrosion of the current collectors [5]. R_{CT} has a huge increase although it has some inconsistent behavior at low cycles. Other charge-transfer region parameters exhibit some inconsistencies as well which may be due to the poor fitting performance of the CNLS at the first data points of the impedance curve (Fig. 7). The suppression factors are remaining relatively constant which is desired as they are regarded to have no practical relation to battery electrochemical phenomena. At SEI region, C_{SEI} shows very minor increase while R_{SEI} is reduced at the beginning of the WLTC cycles. The effect may be caused by the fact that the SEI layer formation is not consistent but taking place at local spots at the surface of the electrodes [4]. In addition, it can be an indication of the lithium-plating effect which is also affecting the SEI region impedance [5].

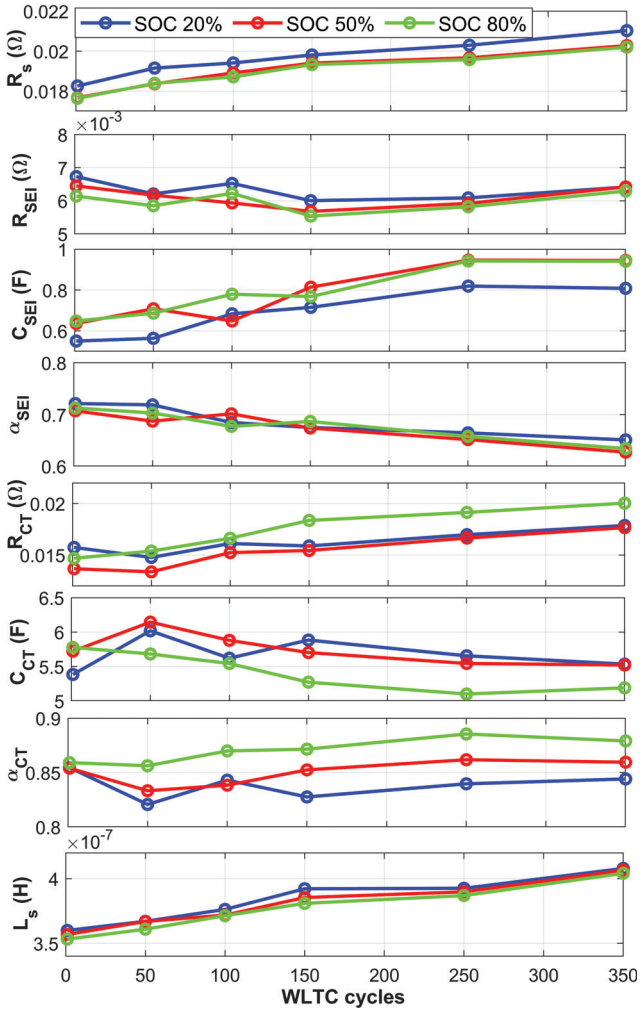

Fig. 8: Fitted ECM parameters at various SOCs as a function of WLTC cycles

The relative changes in the ECM parameters and in the SOH at 50% of SOC are shown in Fig. 9. The linearly changing series resistance and inductance values indicate that the corrosion of the current collectors is affecting rather linearly to the SOH of the battery. The SEI-region resistance is reduced approximately up to 150 cycles and starts to increase at higher cycles. Similar behavior of SEI-region resistance is also reported in [17]. This states that the SEI region impedance is not consistently increased during the battery life. On the other hand, the SEI region behavior may be a consequence of the non-linearity of the ECM and the fact that the width of the SEI region semicircle is included in other resistance R_{s} and R_{CT} in the ECM. This can be reason why the greatest increase is realized for R_{CT} as lithium plating effects usually affecting to R_{CT} is taking place at significantly lower temperatures than what was used for the experiments. The most drastic reduce in the battery capacity is taking place between 250 and 350 cycles where R_{SEI} shows the highest increase. This may indicate

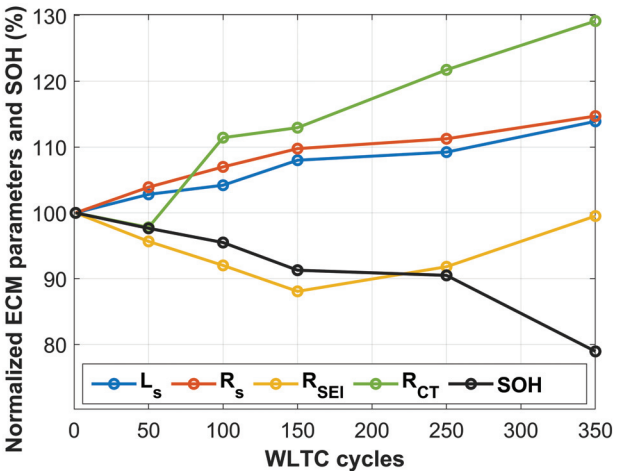

Fig. 9: Beginning-of-life normalized ECM parameters during WLTC cycling at 50% of SOC

that the SEI-layer formation becomes constant throughout the electrode surface as the battery performance starts to drop. Moreover, the increase in R_{SEI} can be observed before the SOH is rapidly reducing. Therefore, the increase in R_{SEI} can be a valuable anticipatory indicator of the drastic capacity and SOH drop in the battery.

VII. Conclusions

This paper has demonstrated the use of PRS impedance measurements technique to track the SOH evolution of the Li-ion NMC battery cell. The battery cell was cycled at 25°C with the WLTC profile to provide a realistic current profile for the analysis. During the cycling, the battery performance was tested with capacity measurements and fast DST signal impedance measurements. The measured impedances were fitted to the ECM by the CNLS algorithm with adaptively obtained initial conditions. The results showed that the ECM was accurately fitted to the impedance data and many of the ECM parameters were changing as the battery SOH reduced. In particular, it was observed that the increase in the SEI region resistance can indicate the upcoming drastic reduction in the battery capacity. The most consistent behavior with respect to the SOH degradation was concluded in the series resistance and inductance parameters of the ECM. The presented methods can be used as an efficient real-time tool for reliable SOH estimation in on-board battery applications.

References

[1] S. Vazquez, S. M. Lukic, E. Galvan, L. G. Franquelo, and J. M. Carrasco, "Energy Storage Systems for Transport and Grid Applications," *IEEE Trans. Ind. Electron.*, vol. 57, no. 12, pp. 3881–3895, 2010.

[2] J. Meng, M. Ricco, G. Luo, M. Swierczynski, D. Stroe, A. Stroe, and R. Teodorescu, "An overview and comparison of online implementable soc estimation methods for lithium-ion battery," *IEEE Transactions on Industry Applications*, vol. 54, no. 2, pp. 1583–1591, March 2018.

[3] M. Berecibar, I. Gandiaga, I. Villarreal, N. Omar, J. Van Mierlo, and P. Van den Bossche, "Critical review of state of health estimation methods of Li-ion batteries for real applications," *Renewable and Sustainable Energy Reviews*, vol. 56, pp. 572–587, apr 2016.

[4] J. Vetter, P. Nov, M. R. Wagner, and C. Veit, "Ageing mechanisms in lithium-ion batteries," *Journal of Power Sources*, vol. 147, pp. 269–281, 2005.

[5] C. Pastor-Fernández, K. Uddin, G. H. Chouchelamane, W. D. Widanage, and J. Marco, "A Comparison between Electrochemical Impedance Spectroscopy and Incremental Capacity-Differential Voltage as Li-ion Diagnostic Techniques to Identify and Quantify the Effects of Degradation Modes within Battery Management Systems," *Journal of Power Sources*, vol. 360, pp. 301–318, aug 2017.

[6] D. I. Stroe, M. Swierczynski, A. I. Stan, V. Knap, R. Teodorescu, and S. J. Andreasen, "Diagnosis of lithium-ion batteries state-of-health based on electrochemical impedance spectroscopy technique," in *2014 IEEE Energy Conversion Congress and Exposition (ECCE)*, Sept 2014, pp. 4576–4582.

[7] M. Petzl, M. Kasper, and M. A. Danzer, "Lithium plating in a commercial lithium-ion battery – A low-temperature aging study," *Journal of Power Sources*, vol. 275, pp. 799–807, feb 2015. [Online]. Available: https://linkinghub.elsevier.com/retrieve/pii/S0378775314018928

[8] A. Lasia, *Electrochemical Impedance Spectroscopy and its Applications*. New York, NY: Springer New York, 2014.

[9] K. Godfrey, *Perturbation Signals for System Identification*. Prentice Hall, 1993.

[10] K. Godfrey, H. Barker, and A. Tan, "Ternary input signal design for system identification," *IET Control Theory & Applications*, vol. 1, no. 5, pp. 1224–1233, sep 2007.

[11] A. H. Tan, "Direct synthesis of pseudo-random ternary perturbation signals with harmonic multiples of two and three suppressed," *Automatica*, vol. 49, no. 10, pp. 2975–2981, oct 2013.

[12] P. Vyroubal and T. Kazda, "Equivalent circuit model parameters extraction for lithium ion batteries using electrochemical impedance spectroscopy," *Journal of Energy Storage*, vol. 15, pp. 23–31, feb 2018.

[13] S. M. M. Alavi, C. R. Birkl, and D. A. Howey, "Time-domain fi tting of battery electrochemical impedance models," *Journal of Power Sources*, vol. 288, pp. 345–352, 2015.

[14] S. M. R. Islam and S.-y. Park, "Circuit Parameters Extraction Algorithm for a Lithium-Ion Battery Charging System Incorporated with Electrochemical Impedance Spectroscopy," *2018 IEEE Applied Power Electronics Conference and Exposition (APEC)*, pp. 3353–3358, 2018.

[15] J. Sihvo, T. Roinila, T. Messo, and D.-i. Stroe, "Novel online fitting algorithm for impedance-based state estimation of Li-ion batteries," in *IECON 19 Proceedings (Industrial Electronics Conference)*. IEEE, 2019.

[16] D. M. Bates and D. G. Watts, Eds., *Nonlinear Regression Analysis and Its Applications*, ser. Wiley Series in Probability and Statistics. Hoboken, NJ, USA: John Wiley & Sons, Inc., Aug 1988.

[17] X. Wang, X. Wei, and H. Dai, "Estimation of state of health of lithium-ion batteries based on charge transfer resistance considering different temperature and state of charge," *Journal of Energy Storage*, vol. 21, no. November 2018, pp. 618–631, 2019.

[18] P. Manganiello, G. Petrone, M. Giannattasio, E. Monmasson, and G. Spagnuolo, "Fpga implementation of the eis technique for the online diagnosis of fuel-cell systems," in *2017 IEEE 26th International Symposium on Industrial Electronics (ISIE)*, June 2017, pp. 981–986.